22

Improved Properties of Optical Surfaces by Following the Example of the "Moth Eye"

Theobald Lohmueller[1,2,3], Robert Brunner[4] and Joachim P. Spatz[1,2]
[1]*Max Planck Institute for Metals Research, Stuttgart, Germany*
[2]*Heidelberg University, Germany*
[3]*Current address: University of California, Berkeley, USA*
[4]*Carl Zeiss AG, Jena, Germany*

1. Antireflective Surfaces - The "Moth Eye" Principle

The versatile visual systems of animals are intriguing examples for the ingenuity of nature's design. Complex optical conceptss evolved as a result of adaptation of individual species to their environment. Identifying innovative applications for modern optics from the broad biological repertoire requires two steps: First, to understand how a system works and second, appropriate process technology to reproduce nature's design on non-living matter. A concrete example of this concept is the antireflective surface found on the eyes of certain butterfly species. The compound eyes of these insects are equipped with a periodic array of sub-wavelength structured protuberances. This structure, referred to as "Moth eye" structure after the moths were it was observed for the first time, thereby reduces reflection, while transmission of the chitin-lens is increased. The evolutionary benefit for the moth is improved vision in a dim environment while chances to be seen by a predator are lowered.
But reflection of light at optical interfaces is also a problem for many technological applications (Kikuta *et al.* 2003). The reflection loss at a single air-glass interface is about 4 % due to the abrupt change of the refractive index. In state-of-the-art lithography systems and microscope devices, with dozens of lenses incorporated, losses of untreated surfaces would add up resulting in a substantial decrease of the overall performance. In the case of semiconductors, reflectance can reach up to 40% due to high refractive indices of the materials (Singh 2003), with impact on the efficiency of solar cells and optoelectronic devices (Partain 1995). Disturbing light reflection from computer monitors, television screens and LCD displays are further examples from daily experience.
Antireflection coatings are most frequently single or multilayer interference structures with alternating high and low refractive indices (Walheim *et al.* 1999) (Sandrock *et al.* 2004) (Xi *et al.* 2007). Reflection is reduced for normal incidence due to destructive interference of reflected light from the layer-substrate and the air-layer interface. However, there are factors limiting the applicability of layer systems like radiation damage and adhesion problems due to different thermal expansion coefficients of substrate and coating material. This is a particular problem for high-power laser applications. State-of-the-art optical lithography for example employs exposure wavelengths in the deep-ultraviolet (DUV) range in order to

address manufacturing demands for high-resolution processing (Chiu *et al.* 1997; Holmes *et al.* 1997). Coatings in this spectral range are difficult to implement, extremely expensive, and only a limited number of materials meet the optical requirements (Ullmann *et al.* 2000; Dobrowolski *et al.* 2002; Kikuta *et al.* 2003; Kaiser 2007).
"Moth eye" surfaces may offer an intriguing solution for these problems: They were first discovered by Bernhard (Bernhard 1967), who proposed that the function of these 'nipple arrays' might be the suppression of light reflection from the eye of the insect in order to avoid fatal consequences for the moth. The origin of these antireflective properties emerge from a gradation of the refractive index between air and the cornea surface (Clapham *et al.* 1973; Wilson *et al.* 1982). SEM micrographs of the surface structure of a genuine moth are shown in Figure 1.

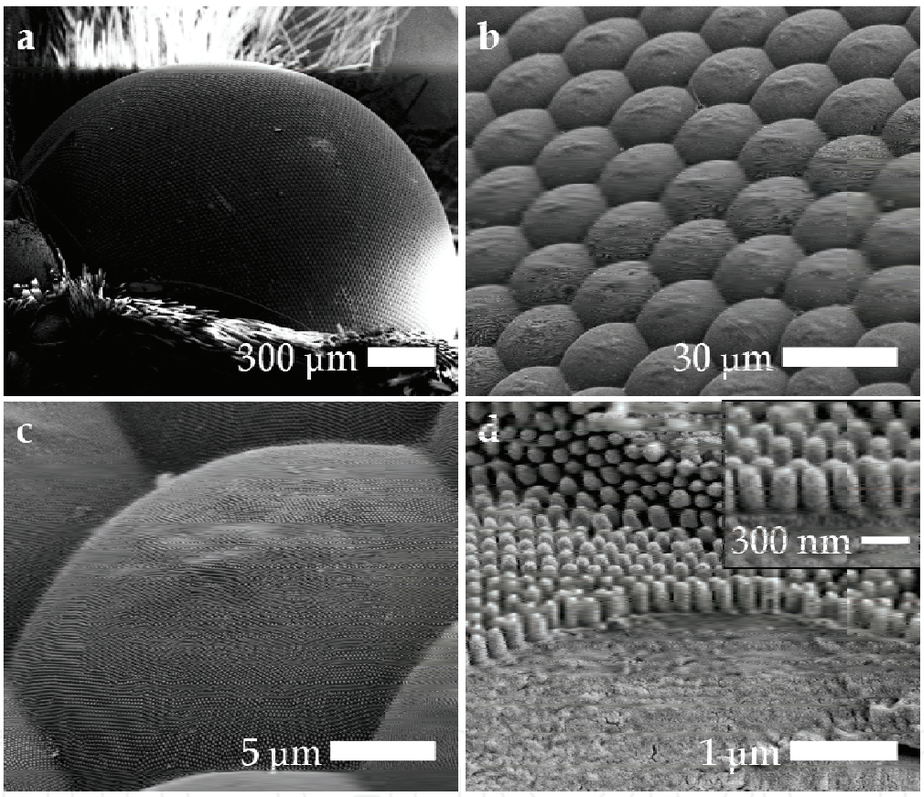

Fig. 1. SEM micrographs of the surface of a genuine moth eye. The compound eye of insects consists of an arrangement of identical units, the ommatidia. Each ommatitdia itself represents an independent optical system with its own cornea and lens to focus light on the subjacent photoreceptor cells. a,b Compound eye of a moth build up by a microlens array of several thousand single lenslets. c, d, The surface of a single ommatidia is equipped with a fine nanoscopic array of protuberances. A detailed overview of structural properties for different butterfly species can be found in literature (Stavenga *et al.* 2006).

Since the distance between the pillars is sufficiently small, the structure cannot be resolved by incident light. Transition between the air-material interface thus appears as a continuous boundary with the effect of decreased reflection and improved transmittance of all light with a wavelength larger than the spacing period. The "Moth-eye" approach has thereby an

advantage compared to state-of-the-art antireflective coatings: Common single- and multi-layer configurations are only applicable within a small wavelength range and near to normal incidence of light. "Moth-eye"-structured surfaces, in contrast, show reduced and angle-independent reflectance over a broad spectral bandwidth (Clapham *et al.* 1973).
In this chapter we want to discuss the physical origin of these exceptional properties and how they can be transferred to optical functional materials. We used metallic nanoparticles as a lithographic mask to generate a quasi-hexagonal pattern of hollow, pillar-like protuberances into glass and fused silica substrates. We report on a combination of self-assembly based nanotechnology and reactive ion etching as a cost-effective and straightforward way for the fabrication of moth-eye inspired interfaces fully integrated in the optical material itself. The structures were found to exhibit broadband antireflective properties ranging from deep-ultraviolet to infrared light at oblique angles of incidence (Lohmueller *et al.* 2008b).

2. Theoretical Considerations

According to their complexity antireflection coatings can be classified by two basic models. Reduced reflectance can either be achieved by a homogeneous single-layer or digital type coating or by a more complex inhomogeneous multilayer configuration or gradual profile pattern respectively, that provides a gradual refractive index transition at the air/material interface (Dobrowolski *et al.* 2002).In the simplest case, a single homogeneous layer with a refractive index n will suppress reflectance between a substrate n_s and air n_a for normal incidence of light and an optical thickness of $\lambda/4$, if the constraint $n = (n_s\, n_a)^{0.5}$ is fulfilled. The demand for $\lambda/4$ thickness is based on both effects, the optical path difference and also the phase change at the low-to-high refractive index interface. It is important to point out that such configurations are always limited to a single wavelength.
An improvement is achieved by the introduction of multilayer systems which show an increased but still limited spectral bandwidth and also allow only a narrow variation of the incidence angle. Further optimizations are possible by using gradient optical coatings which show broadband antireflective characteristics for omnidirectional incidence of light (Poitras *et al.* 2004).The first theoretical description of this characteristic was published by J. S. Rayleigh in 1880, who mathematically demonstrated the broadband antireflection properties of graded-refractive index layers (Rayleigh 1880). For a discontinuous boundary the reflection coefficient at the interface of two media can be expressed as (Wilson *et al.* 1982)

$$R = [(n_1 - n_2)/(n_1 + n_2)]^2 \tag{1}$$

where n_1 and n_2 are the refractive indices. For a series of refractive indices, the total reflectance is a result of the interference of all reflections at each incremental step along the gradient. Each reflection has a different phase, as they come from a different depth of the substrate. The overall reflectance will therefore be suppressed, if the height of the antireflective structure equals to $\lambda/2$ and all phases are present.
In case of the "Moth eye" surface, the quasi periodical structure of the protuberances is characterized by a lateral period which is much smaller than the optical wavelength. The structure thus acts as a diffraction grating where only the zeroth order is allowed to propagate and all other orders are evanescent. The "moth eye" cornea is optically equivalent

to a laterally nonstructured film with a gradual change of the refractive index in depth. Figure 2 shows schematically the continuous increase of the physical thickness along the antireflective structure from air to bulk.

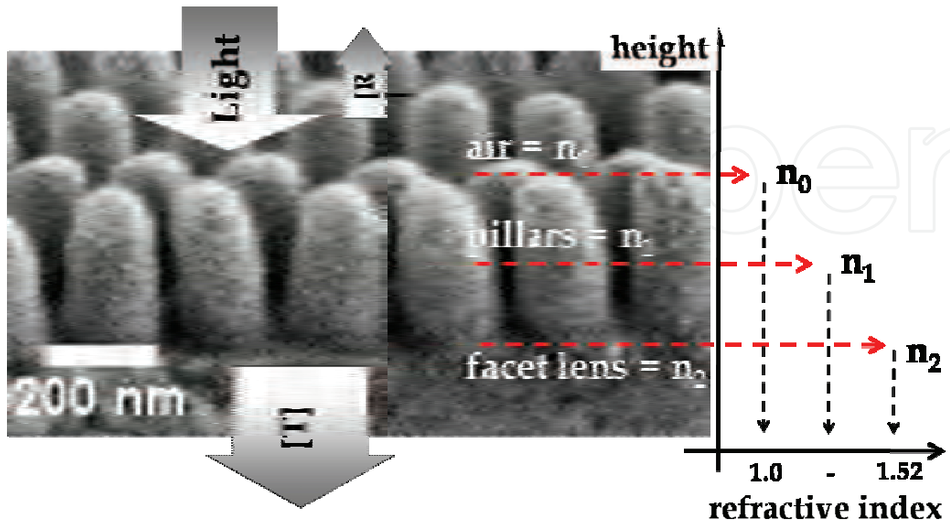

Fig. 2. Effective refractive index profile of a genuine moth eye. The fine array of protuberances on the lens of an insect eye has a structural period, smaller than the wavelength of the incoming light. This special profile is leading to a gradient increase of the material density and thus the refractive index at the air-cornea interfaces responsible for the antireflective properties.

This model of gradual index change is also the underlying principle for various effective medium approaches with the intention to introduce numerical methods which allow the determination of the dielectric constant of subwavelength structured composite materials (Lalanne *et al.* 2003). These approaches, however, represent only a rough approximation of the reality with a poor account for the individual profile geometry, especially if the structural period is infinitely smaller than the wavelength. A more exact form is given by the effective medium theory (EMT). Considering a 1D periodic structure with a gradual index profile, the effective refractive index n_{eff} of the whole interface can be expanded in a power series according to (Lalanne *et al.* 1996):

$$n_{eff} = n^{(0)} + n^{(2)}(\Lambda/\lambda)^2 + n^{(4)}(\Lambda/\lambda)^4 + \ldots \quad (2)$$

Here, $n^{(0)}$ represents the effective index in the long-wavelength limit $n^{(2)}$ and and $n^{(4)}$ are dimensionless coefficients depending on the structural geometry. Λ/λ denotes the period-to-wavelength ratio between the grating period of the 1D profile and the respective wavelength. While closed-form expressions like equation (2) are feasible up to the fourth order, an exact expression of n_{eff} for 2D periodic structures, like the moth eye, has not been achieved.

Alternatively, rigorous coupled wave analysis (RCWA), represents a method for the numerical calculation and simulation of light waves, as they are propagating in periodic media. The RCWA thereby represents an approximation of the Maxwell Equations

(Moharam *et al.* 1981). For RCWA, the geometry of a periodic pattern is divided into a define number of incremental optical layers. This stack region represents a transition between two semi-infinite regions such as air and the substrate. The light propagation is now calculated by the interaction of the incoming electromagnetic field with the layer stack where especially mutual interdependency has to be taken into account. The surface profile of a nanopatterned optical interface can thus be modeled by dividing the structure in a sufficiently small number of stack layers where each layer has a higher filling factor (and a higher optical thickness, respectively) than the previous one. The RCWA approach can be extended to accurately calculate the optimum surface-relief profile with respect to the refractive index of the material. Southwell et al. showed that the side-walls of a pyramid-like gradient profile would have an optimum shape (and thus optimum antireflective properties), for a fifth-order (quintic) functional dependence of the refractive index on the optical thickness (Southwell 1983; Southwell 1991):

$$n = n_s - (n_s - 1)(10u^3 - 15u^4 + 6u^5) \tag{3}$$

where u denotes the normalized optical thickness of the material ranging from zero at the dense substrate to unity at the air/substrate interface. The optimum slope of the pyramid sidewalls is thereby depending on the refractive index of the medium. Calculating the quintic surface profile reveals that curved, rather than flat-sided pyramids result in an index-matching layer with optimum antireflective properties at dielectric interfaces (Southwell 1991).

3. Subwavelength Structured Optical Interfaces

3.1 Fabrication of Artificial "Moth Eye" Structures

Different techniques such as e-beam writing (Kanamori *et al.* 1999; Kanamori *et al.* 2000; Toyota *et al.* 2001), mask lithography (Motamedi *et al.* 1993), and Interference Lithography (Gombert *et al.* 1998) have been applied to realize master structures for sub-wavelength structured gratings. To avoid scattering from the optical interface, the structural dimensions have to be smaller than the wavelength of the incoming light ('lower wavelength limit') (Wilson *et al.* 1982; Southwell 1991; Dobrowolski *et al.* 2002). For UV and DUV applications, very small feature sizes below 200 nm are required. At the same time, the overall reflectance is a function of the AR-layer thickness d and the wavelength λ (Rayleigh 1880). For a graded-index transition, substantial anti-reflection is obtained, if the ratio d/λ is about 0.4 or higher (Wilson *et al.* 1982; Lalanne *et al.* 2003). Thus, for optimum anti-reflection conditions in the DUV region the height of the structure should be at least 100 nm. In this size range, conventional fabrication technologies suffer from being time-consuming, expensive and rather complicated. Moreover, processing of non-planar substrates like lenses, especially with a small radius of curvature is challenging. An alternative is offered by self-assembly based methods. Porous alumina membranes (Kanamori *et al.* 2001) or block copolymer layers were used in combination with subsequent dry-etching (Park *et al.* 1997; Cao *et al.* 2003) (Asakawa *et al.* 2002). In the latter example, the etch selectivity between acrylic and aromatic polymer components results in a surface topography of the underlying material. Structure depths between 8 and 30 nm have been reported in silicon, too thin to obtain a substantial anti-reflective effect. Alternative approaches like porous sol-gel (Thomas 1992),

and optical polymer thin film coatings (Walheim *et al.* 1999; Ibn-Elhaj *et al.* 2001) are not useful for UV applications.

Colloidal monolayers of SiO_2 and polystyrene spheres have also been used in a combination with reactive ion etching (RIE) to lower the substrate reflectance (Nositschka *et al.* 2003) (Cheung *et al.* 2006) but the fabrication of small nanostructures below 200 nm covering large surface areas is challenging. An alternative route is offered by rough metal films or colloidal gold particles as masking material (Lewis *et al.* 1998) (Lewis *et al.* 1999; Seeger *et al.* 1999; Haupt *et al.* 2002). The etch mask in these examples is placed on top of silicon wafers by either sputter coating of metal islands or random deposition of colloidal gold particles out of solution. Stochastic relief structures with a spatial resolution smaller than 100 nm have been realized but both methods do not allow control of structural parameters such as feature size and spacing.

We applied Block Copolymer Micelle Nanolithography (BCML) in order to create extended and highly ordered arrays of gold nanoparticles on optical functional materials like fused silica and glass by means of pure self assembly (Spatz *et al.* 2000; Glass *et al.* 2003). Polystyrene-block-poly(2)-vinylpyridine, (PS-b-P2VP) diblock copolymers were dissolved in toluene forming uniform spherical micelles. Tetrachloroaurate, $HAuCl_4$ was added to the solution with a stoichiometric loading parameter defined as L = n[Me]/n[P2VP] (Me = metal salt), in order to neutralize the vinylpyridine block, which mainly represents the micellar core. After stirring for 24 h, all metal salt is dissolved. Glass cover slips (n = 1,52) and fused silica wafers (n = 1,46) are immersed into solution. During the retraction, a self-assembled monolayer of metal salt loaded micelles is formed on top of the substrate driven by the evaporation of the solvent. Dipping the substrate has a certain advantage over other methods in that it enables a fast and homogeneous coating of plane as well as curved substrates like e.g. lenses with high reproducibility. BCML has no special requirements for the substrate composition besides it has to be resistant to the solvent. The polymer matrix is entirely removed by hydrogen plasma treatment of the sample leaving a template of hexagonally ordered gold particles on the surface. Various materials such as glass, silica, GaAs, mica as well as saphire or diamond can be completely structured with nanosized particles over a large area >> cm^2 within minutes. Advantageous of this technique is that the interparticle distance and the average colloidal diameter can be adjusted independently of one another enabling particle spacing between 15 and 250 nm and a precise control of the particle size (Lohmueller *et al.* 2008a). These particles act as a shadow mask for subsequent reactive ion etching (RIE) leading to a surface texture with anti-reflective properties (Figure 3).

We realized antireflective nanostructures on glass and on both, plane and biconvex fused silica surfaces. The structural period was set to 100 nm with a structure depth between 60 nm and 120 nm.

The gold nanoparticles are functioning as a protective resist during the etching process due to their high stability against the plasma treatment compared to the underlying material. Since the RIE process represents an unselective physical ion bombardment of the sample, the gold particles are continuously reduced in size until they are used up completely. From that moment on, the whole surface is uniformly etched and the structure is destroyed. Artificial moth eye structures were prepared on glass and fused silica as shown in Figure 4.

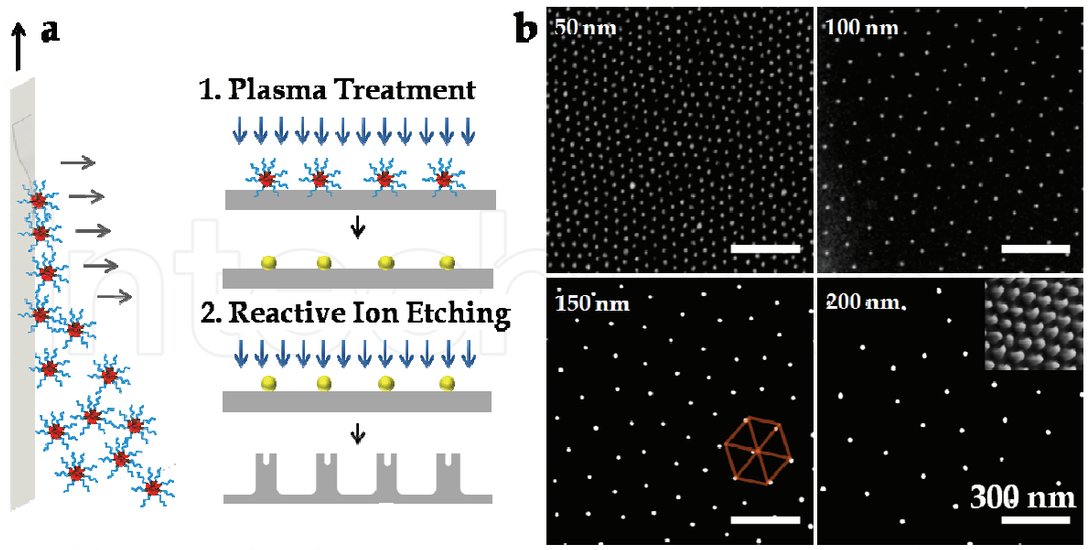

Fig. 3. Schematic of the fabrication process. a, The substrate is immersed into a toluene solution of metal salt loaded micelles. During retraction, a micellar monolayer self-assembles on top of the substrate driven by capillary forces due to the evaporation of the solvent. The polymer matrix is removed entirely by hydrogen plasma treatment and results in the deposition of an extended array of elemental gold particles on top of the substrate. Gold nanoparticles act as an efficient mask for etching hollow cone-like pillars into the underlying silica support by Reactive Ion Etching (RIE). b, The distance between the nanoparticles can be controlled over several hundreds of nanometers. The hexatic arrangement of the particles on the surface is similar to the orientation of the protuberances found on the eye of moths.

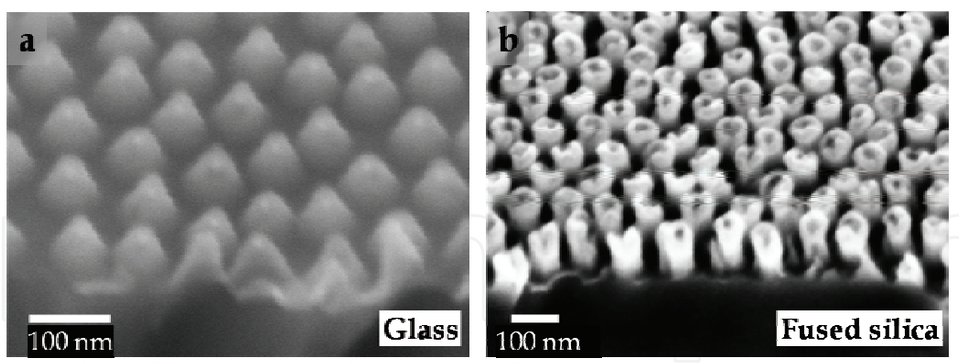

Fig. 4. "Moth-eye" structured glass cover slips and fused silica samples. a, High magnification micrograph showing the triangular shape of the glass cones. b, Side-view image of the pillar array measured with a tilt angle of 45°

The nanostructure profiles were different depending on the substrate material. On the glass-cover slips, the process resulted in a homogeneously patterned array of nano-cones with a diameter of 80 ± 5 nm at the base and a structural depth of app. 60 nm, representing the effective thickness of the antireflective layer. The sidewalls of the cones had an inclination angle of app. θ= 60°. The triangular shape found on top of the normal glass is a consequence

of a mixed isotropic-anisotropic etching at a moderate plasma power with an etch rate of app. 10 nm/min. According to theory, the optimum quintic profile for glass corresponds to the form of a nearly flat sided pyramid (Southwell 1991). Therefore, the process values were elaborated in order to generate an array of glass cones, which continuously converge towards the bottom. The sharp cone tips are indicating the optimum etching time. The samples were processed until the colloidal metal spheres were completely removed. For longer sample processing or higher RF power, the tips of the structure are blunted and the height is reduced. In both cases the optical performance declines considerably.). For fused silica, a rather anisotropic etch profile was observed with an etch rate of 30 nm/min, three times higher than in the case of normal glass. Instead of sloping side walls, the structure had a vertical, pillar-like shape with a diameter of 60 ± 8 nm and a lateral spacing of 114 ± 3 nm (center to center) respectively. The different result can be explained by the lower resistance of the fused silica against the plasma treatment compared to normal glass. The height of the structure was measured to be 120 nm, which corresponds to the effective thickness of the antireflective layer (Figure 5).

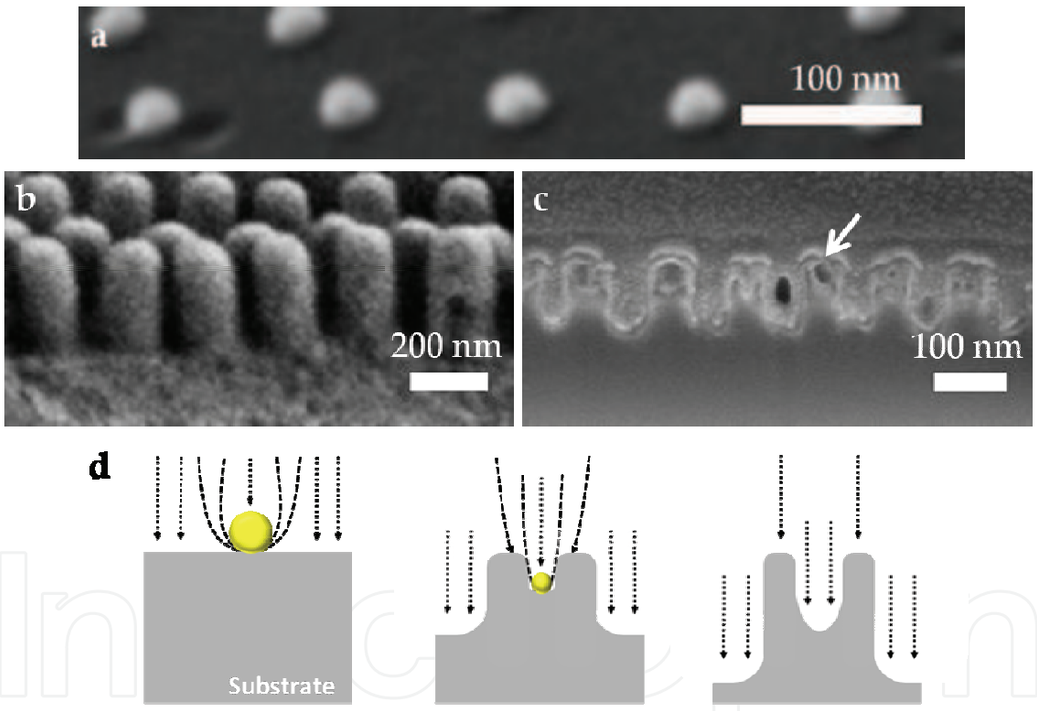

Fig. 5. a, 60° side-view SE-micrograph of the gold nanoparticles used as an etch mask. Comparison between a cross section of the cornea of a b, moth eye and the c, artificial moth eye profile in fused silica. Focused Ion Beam (FIB) cross section through the antireflective structure. The pillars have a diameter of 60±4 nm and a lateral spacing of 110±7 nm (center to center), respectively. The height of the structure was measured to be 120±5 nm which corresponds to the effective thickness of the antireflective layer. A cone-type hole is etched into each pillar tip to approximately half of the pillar height. e, Schematic displaying the fabrication of hollow cone-like pillars during the reactive ion etching process in the presence of gold nanoparticles.

Remarkably, the tips of the pillars are hollow and pores are formed at the spots where the gold particle had been placed originally. A hole is etched into each pillar tip to app. half of the pillar height. This is caused by a electrostatic sheath ("Debye Sheath") (Langmuir 1923; Hull *et al.* 1929), formed above the sample during the plasma process (Figure 5 d). In the sheath region a strong electric field is generated perpendicular to the surface. The presence of electrical conductive gold clusters on top of the insulating material, however, causes a sheath distortion in the vicinity of the conductor/insulator interface (Kim *et al.* 2004). The reactive ions of the plasma are thereby focused to the contact area of the metallic nanoparticles with the underlying fused silica substrate. This causes a depletion of the plasma-generated reactive ion concentration around the metal islands. As a consequence, the particles act as an etching mask for processing hollow, cone-like pillars oriented perpendicular to the substrate. During the etching process, the particles sink into the material and the particle diameter continuously decreases until they are completely used up. The outer diameter of the pillars is larger than the nanoparticles due to depletion of ion concentration, while the inner diameter of the hollow structure reflects the original particle size. As mentioned earlier, a gradual increase of material from air to bulk is responsible for the substrate's anti-reflection properties (Moharam *et al.* 1981) (Kikuta *et al.* 2003). Consequently, the partly hollow, cone-type pillars are expected to improve the anti-reflective quality of the structure.

3.2 Optical Characterization

Different sub-wavelength profiles were obtained depending on the substrate material showing significant anti-reflective properties over a broad wavelength range from the deep UV up to the IR region. The optical properties of the fabricated samples were investigated by wavelength dependent transmission measurements. The incidence direction of the probe beam was oriented perpendicular to the surface. An unstructured substrate was measured in each case as a reference. For quantification, the reference measurement was also used to subtract the reflex from the backside of the single-sided structured samples. Figure 6 shows the measured transmission in dependence on the wavelength for glass and fused silica.

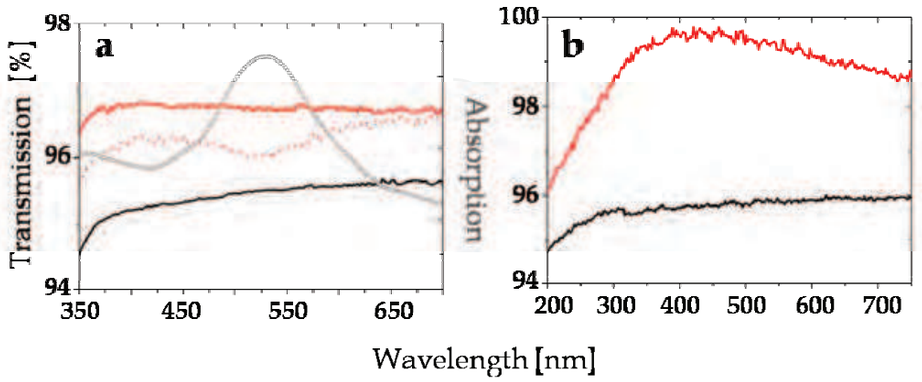

Fig. 6. Transmittance of an untreated and sntireflective structured substrate of a, glass and b, fused silica. Residuals of the gold particles are visible in the spectra by a minimum of the transmission curve (red dotted line) that correlates with the maximum of the absorbance spectra (grey line) of the plasmon resonance of the gold particles. The reflex contribution of the sample backsides was subtracted for all spectra.

The distinct antireflective properties are clearly observable over the whole observed spectral region. Increased transmission of nearly 2% at a wavelength of 350 nm was detected compared to a reference glass cover slip. Residual gold may be left over on top of the substrate after RIE. However, if there are any remains of the particles, they are visible in the transmission spectrum. This is shown in Figure 6 a by the curve minimum that appears around 530 nm overlapping with the maximum of the absorbance spectra that was taken from the same sample. After five minutes no vestiges of the gold were detectable. By an alternate measurement of plasmon absorbance and overall transmission it is thus possible to determine the point of time when the particles are completely used off during the RIE process. Beside their role as plasma resist, the gold particles are thereby acting as an indicator for the course of the experiment. The transmission efficiency for the pillar-like structures was higher compared to the cone-shaped profile found on the glass cover slips. The reason is the smaller height of the glass indentations of only 60 nm, where the fused silica samples reached a structural depth of up to 120 nm. The effective thickness of the structure is mainly responsible for the efficiency of the antireflective properties and should therefore be in the order of half the wavelength or more. In the case of the VIS spectral region, ideal structure depth would therefore be between 200 nm and 400 nm. The desired parameters for an artificial moth eye design imply a structural spacing as small as possible and a structural depth as great as possible to achieve the least reflection and highest transmission over a broad bandwidth. The obtained pillar height, however, should show an optimum performance for the aspired wavelength range below 300 nm. The topology of the fused silica sample was similar to the corneal surface of a real moth.

As already mentioned, the moth eye lens shows a superior optical performance compared to many non-natural materials, since the overall reflection is reduced, while at the same time the transmission of light in the visible range is increased for omni-directional incidence of light. This is in contrast to non-reflecting coatings based on compound films or unspecific surface roughness, where diffuse scattering reduces the reflection but transmission is damped at the same time. The optical properties of plane fused silica samples were investigated by angle dependent reflection measurements at a particular as shown in Figure 7.

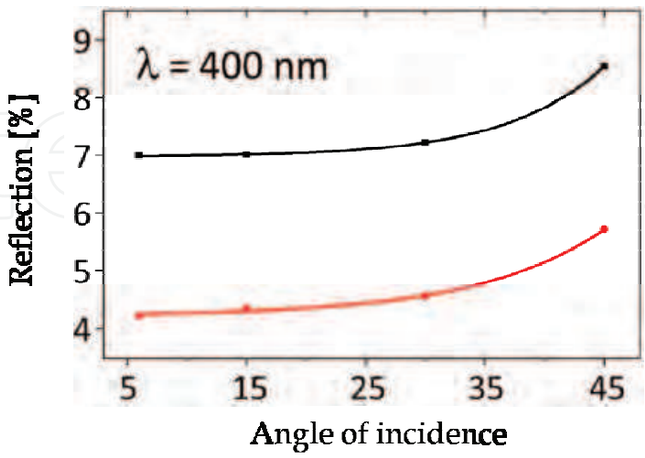

Fig. 7. Reflectance of an antireflective structured (red line) and a reference (black line) sample as a function of incident angle. The reflex contribution of the sample backsides was not subtracted in this case.

An increase of the total transmission was observed over a spectral range from 300 to 800 nm. At λ = 400 nm the transmittance reached a maximum value of 99.3 % (Figure 6 b), while the reflectivity of the same sample was damped to 0.7 %. Since the improved transmission is in accordance with a reduced reflectance, it is apparent that light scattering defects or absorption losses, which might have been introduced by the fabrication process, play, if at all existing, a minor role. The reflection and transmission under a certain angle is dependent on the polarization of the incoming light due to Fresnel's law as demonstrated in Figure 8.

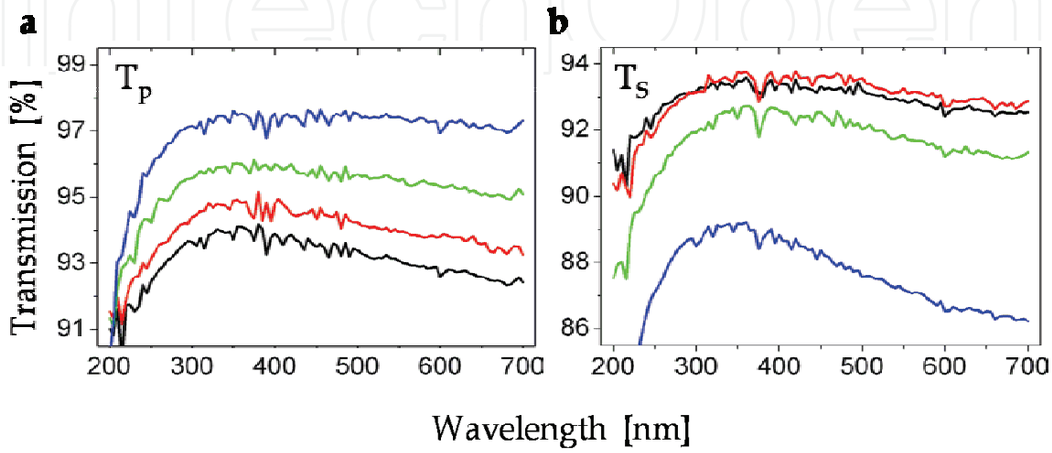

Fig. 8. Angle dependent transmission with polarized light. a,b,Spectral transmission of p- ands-polarized light for different angles of incidence(black: 0; red: 15; green: 30; blue: 45)

As expected, the difference between the transmittance for p - and s - polarized light is increasing towards larger polarization angles with a maximum dispartment at the Brewster angle (55.4° for fused silica, n = 1.46) (Hecht 2002).

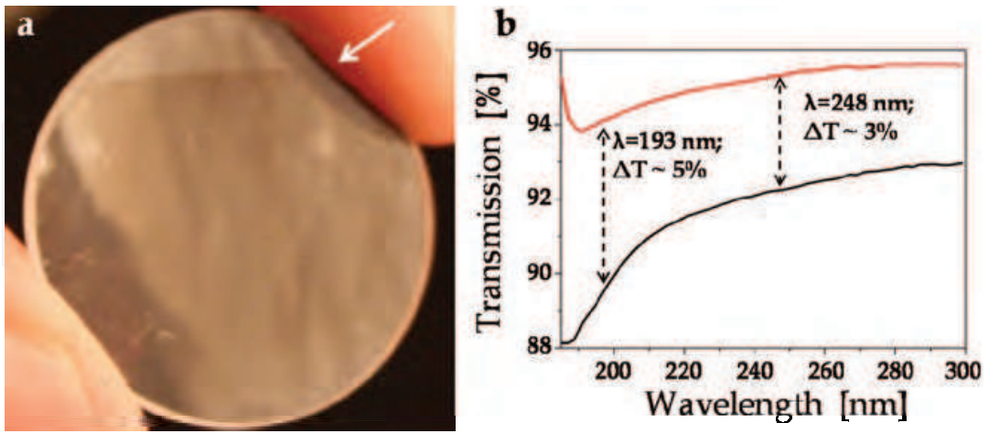

Fig. 9. Optical properties of an antireflective structured lens. a, Photograph of the processed lens demonstrating the anti-reflective effect. The borderline between the structured (bottom) and unstructured (top) area is indicated by the white arrow. b, Transmission spectra of the same lens before (black line) and after (red line) processing. An increase of transmission was observed for the DUV range from 185 to 300 nm. The improved transmission values for the excimer laser wavelengths 193 nm (ArF) and 248 nm (KrF) are shown exemplary.

To demonstrate the excellent applicability of the method to non-planar optical components, the convex side of a fused silica lens was processed and characterized by sub-300 nm transmission measurements. The planconvex lens had a diameter of 22.4 mm and a focal distance of 100 mm, which corresponds to a radius of curvature of 46 mm. The reduced reflectivity in the visible light region of the structured part of the lens surface is shown in Figure 9. More intense light reflectivity is seen above the line indicated by the white arrow which is the border line between the nanostructured and the unstructured part of the lens surface, whereas, the antireflective structured part of the lens appears less bright.
Transmission in the DUV range was measured between 185 and 300 nm (Figure 9b). The performance was improved over the entire DUV spectral region, by 5 % for 193 nm and 3 % for 248 nm at the excimer laser wavelengths of ArF and KrF, respectively. The high increase of transmission of about 5 % therefore relate to a virtual elimination of reflection at the modified optical interface.

3.3 Wettability of Nanostructured Interfaces

Beside the improved optical performance, a substantial change of the surface wettability was observed for the antireflective structured fused silica samples. This observation is advantageous, since an additional self-cleaning property of the optical interface would even enhance its practical applicability. Contact angle measurements were performed to investigate the hydrophopic effect of the antireflective structured fused silica interface. A difference of the contact angle of about 100° was observed between a plain and structured fused silica sample, which is a clear change of the surface wettability from hydrophilic to hydrophobic as shown in Figure 10.

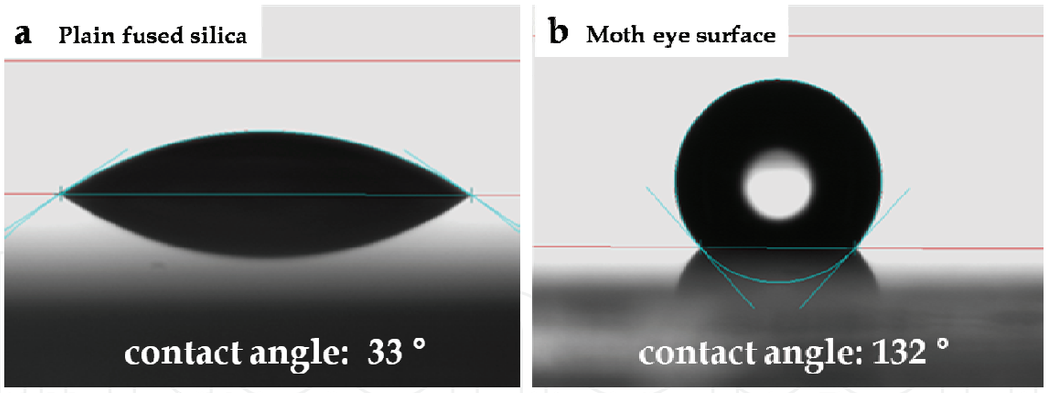

Fig. 10. Wetting of "Moth-eye" nanostructured fused silica samples. The contact angle for water of a, plane and b, nanostructured fused silica samples is increased from 33° to 132°.

A famous example for topology induced superhydrophobicity is the lotus effect (Neinhuis *et al.* 1997). The leaves of lotus plants, although they usually grow in a swamp like, muddy habitat, stay clean, since a certain microscopic structure and surface chemistry prevent the leaves from being moistened. Instead of a liquid film, water droplets are formed which pick up dirt as they roll of the leave. In contrast to the lotus leaf, no additional change of the surface chemistry was introduced to amplify the water repellent properties. The hydrophopicity in this case is solely a result of the special surface topology. This observation can be explained according to the Cassie's approach of surface wettability on rough

substrates (Cassie 1948). As shown in Figur 5 c the antireflective structure is build up by half-hollow protuberances with steep sidewalls. Grooves between the pillars, as well as the hollow pillar heads are leading to a strong lowering of the water-solid contact area. Furthermore, air bubbles are trapped within the structure forming a material-air-water composite interface. Wetting of the pillar structure is hindered, due to the steep sidewalls and the surface tension of water resulting in a liquid meniscus between the nanoscopic features and a high Laplace pressure. The effect of the sidewall angle α and the Laplace pressure Δp can be expressed according to (Patankar 2003; Xiu *et al.* 2007):

$$\Delta p = p - p_0 = -\frac{\gamma \cos(\theta - \alpha)}{R_0 + h \tan \alpha} \tag{4}$$

In this equation, (denotes the surface tension of water, θ is the contact angle of water on the structure, R_0 is half of the width between two individual pillar sidewalls, p is the pressure on the liquid side of the meniscus and p_0 is the atmospheric pressure. The geometry of the structure is considered in this equation by the inclination angle α perpendicular to the surface. For steep sidewalls α = 0°, the Laplace equation is reduced to:

$$\Delta p = -\frac{\gamma \cos \theta}{R_0} \tag{5}$$

In this state, the Laplace pressure Δp has its highest value for a small R_0 which results in an increase of the water contact angle on top of the substrate.

4. Conclusion

We have demonstrated a new approach for the low-cost fabrication of antireflective structured materials is demonstrated by utilizing the advantage of self-assembly based nanolithography and reactive ion etching. Quasi hexagonal arrays of gold nanoparticles are used as an etch mask for plasma processing of glass cover slips and fused silica wafers. Cone-shaped and pillar-like protuberances with a structural period of 100 nm and a height of 60 nm and 120 nm, respectively, have been fabricated. Anti-reflective properties of these structures were demonstrated by transmission and reflection measurements for wavelengths ranging from deep UV to IR for oblique angles of incidence. Applicability of the fabrication method has been demonstrated on planconvex fused silica lenses with the result of a substantially increased transmittance of light in the DUV spectral region between 185 and 300 nm. Beside the remarkable optical properties, these structures offer additional advantages compared to thin-film coatings in terms of mechanical stability and durability. "Moth eye" structured devices can be used over a broad thermal range since they are essentially free of adhesion problems and tensile stress between the substrate and the antireflective layer. In addition, "Moth eye" structured fused silica samples were found to show a strong hydrophobicity caused by air that is trapped in the grooves between the hollow pillar features and the water-material interface. Overall, the method represents a fast, inexpensive, and very reproducible way for the fabrication of highly light-transmissive, anti-

reflective optical materials to be used for display panels, projection optics and heat-generating microscopic and excimer laser applications.

5. References

Asakawa, K. and T. Hiraoka (2002). "Nanopatterning with microdomains of Block Copolymers using reactive-Ion etching selectivity." Japanese Journal of Applied Physics **41**: 6112-6118.

Bernhard, C. G. (1967). "Structural and functional adaptation in a visual system." Endeavour **26**: 79-84.

Cao, L., J. A. Massey, et al. (2003). "Reactive ion etching of cylindrical polyferrocenylsilane block copolymer micelles: Fabrication of ceramic nanolines on semiconducting substrates." Advanced Functional Materials **13**: 271-276.

Cassie, A. B. D. (1948). "Contact angles." Discussions of the Faraday Society **33**: 11-16.

Cheung, C. L., R. J. Nikoli, et al. (2006). "Fabrication of nanopillars by nanosphere lithography." Nanotechnology **17**: 1339–1343.

Chiu, G. L. T. and J. M. Shaw (1997). "Optical Lithography: Introduction." IBM Journal of Research and Development **41**(1/2).

Clapham, P. B. and M. C. Hutley (1973). "Reduction of lens reflection by the moth eye principle." Nature **244**(3): 281-282.

Dobrowolski, J. A., D. Poitras, et al. (2002). "Toward perfect antireflection coatings: numerical investigation." Applied Optics **41**(16): 3075-3083.

Glass, R., M. Moeller, et al. (2003). "Block copolymer micelle nanolithography." Nanotechnology **14**: 1153-1160.

Gombert, A., K. Rose, et al. (1998). "Antireflective submicrometer surface-relief gratings for solar applications." Solar Energy Materials & Solar Cells **54**: 333-342.

Haupt, M., S. Miller, et al. (2002). "Semiconductor nanostructures defined with self-organizing polymers." Journal of Applied Physics **91**: 6057-6059.

Hecht, E. (2002). Optics, Addison Wesley.

Holmes, S. J., P. H. Mtchell, et al. (1997). "Manufacturing with DUV lithography." IBM Journal of Research and Development **41**.

Hull, A. W. and I. Langmuir (1929). "Control of an arc discharge by means of an grid." PNAS **15**(3): 218-225.

Ibn-Elhaj, M. and M. Schadt (2001). "Optical polymer thin films with isotropic and anisotropic nano-corrugated surface topologies." Nature **410**(6830): 796-799.

Kaiser, N. (2007). "Old rules useful to the designer of optical coatings." Vakuum in Forschung und Praxis **19**(4): 17–23.

Kanamori, Y., K. Hane, et al. (2001). "100 nm eriod silicon antireflection structures fabricated using a porous alumina membrane mask." Applied Physics Letters **78**(142-143).

Kanamori, Y., H. Kikuta, et al. (2000). "Broadband antireflection gratings for glass substrates fabricated by fast atom beam etching." Japanese Journal of Applied Physics **39**: L735-L737.

Kanamori, Y., M. Sasaki, et al. (1999). "Antireflection gratings fabricated upon silicon substrates." Optics Letters **24**: 1422-1424.

Kikuta, H., H. Toyota, et al. (2003). "Optical elements with subwavelength structured surfaces." Optical Review **10**(2): 63-73.

Kim, D. and D. J. Economou (2004). "Simulation of a two-dimensional sheath over a flat insulator-conductor interface on a radio-frequency biased electrode in a high-density plasma." Journal of Applied Physics **95**: 3311-3318.

Lalanne, P. and M. Hutley (2003). Encyclopedia of Optical Engineering - Artificial Media Optical Properties—Subwavelength Scale, Marcel Dekker, Inc.

Lalanne, P. and D. Lemercier-Lalanne (1996). "On the effective medium theory of subwavelength periodic structures." Journal of Modern Optics **43**(10): 2063-2086.

Langmuir, I. (1923). "Positive ion currents from the positive column of mercury arcs." Science **58**(1502): 290-291.

Lewis, P. A. and H. Ahmed (1999). "Patterning of silicon nanopillars formed with a colloidal gold etch mask." Journal of Vaccum Science and Technology B **17**: 3239-3243.

Lewis, P. A., H. Ahmed, et al. (1998). "Silicon nanopillars formed with gold colloidal particle masking." Journal of Vaccum Science and Technology B **16**(6): 2938-2941.

Lohmueller, T., E. Bock, et al. (2008a). "Synthesis of quasi hexagonal ordered arrays of metallic nanoparticles with tuneable particle size." Advanced Materials **20**(12): 2297-2302

Lohmueller, T., M. Helgert, et al. (2008b). "Biomimetic Interfaces for high-performance optics in the Deep-UV light range." Nano Letters **8**(5): 1429-1433

Moharam, M. G. and T. K. Gaylord (1981). "Rigorous coupled-wave analysis of grating diffraction." Journal of the Optical Society of America A: Optics, Image Science, and Vision **71**: 811-818.

Motamedi, M. E., W. H. Southwell, et al. (1993). "Antireflection surfaces in silicon using binary optics technology." Applied Optics **31**(22): 4371-4376.

Neinhuis, C. and W. Barthlott (1997). "Characterization and distribution of water repellent, self-cleaning plant surfaces." Annals of Botany **6**: 667-677.

Nositschka, W. A., C. Beneking, et al. (2003). "Texturisation of multicrystalline silicon wafers for solar cells by reactive ion etching through colloidal masks." Solar Energy Materials & Solar Cells **76**: 155–166.

Park, M., C. Harrison, et al. (1997). "Block Copolymer Lithography: Periodic arrays of ~10^{11} holes in 1 square centimeter." Science **276**: 1401-1404.

Partain, L. D. (1995). Solar cells and their applications, Wiley Series in Microwave and Optical Engineering.

Patankar, N. A. (2003). "On the modeling of hydrophobic contact angles on rough surfaces." Langmuir **19**: 1249-1253.

Poitras, D. and J. A. Dobrowolski (2004). "Toward perfect antireflection coatings. 2. Theory." Applied Optics **43**(6): 1286-1295.

Rayleigh, J. S. (1880). "On reflection of vibrations at the confines of two media between which the transition is gradual." Proceedings of the London Mathematical Society **11**: 51-56.

Sandrock, M., M. Wiggins, et al. (2004). "A widely tunable refractive index in a nanolayered photonic material." Applied Physics Letters **84**(18): 3621-3623.

Seeger, K. and R. E. Palmer (1999). "Fabrication of silicon cones and pillars using rough metal films as plasma etching masks." Applied Physics Letters **74**: 1627-1629.

Singh, J. (2003). Electronic and optoelectronic properties of semiconductor structures, Cambridge University Press.

Southwell, W. H. (1983). "Gradient-index antireflection coatings." Optics Letters **8**(11): 584-586.

Southwell, W. H. (1991). "Pyramid-array surface-relief structures producing antireflection index matching on optical surfaces." Journal of the Optical Society of America A: Optics, Image Science, and Vision **8**(3): 549-553.

Spatz, J. P., S. Moessmer, et al. (2000). "Ordered deposition of inorganic clusters from micellar block copolymer films." Langmuir **16**: 407-415.

Stavenga, D. G., S. Foletti, et al. (2006). "Light on the moth-eye corneal nipple array of butterflies." Proceedings of the Royal Society B: Biological Sciences **273**(1587): 661-667.

Thomas, I. M. (1992). "Method for preparing porous silica antireflection coatings varying in refractive index from 1,22 to 1,44." Applied Optics **34**: 6145-6149.

Toyota, H., K. Takahara, et al. (2001). "Fabrication of microcone array for antireflection structured surface using metal dotted pattern." Japanese Journal of Applied Physics **40**: 747-749.

Ullmann, J., M. Mertin, et al. (2000). "Coated Optics for DUV-Excimer Laser Applications." Proc. SPIE **3902**: 514-527.

Walheim, S., E. Schaeffer, et al. (1999). "Nanophase-separated polymer films as high-performance antireflection coatings." Science **283**: 520-522.

Wilson, S. J. and M. C. Hutley (1982). "The optical properties of 'moth eye' antireflection surfaces." Optica Acta **7**: 993-1009.

Xi, J. Q., M. F. Schubert, et al. (2007). "Optical thin-film materials with low refractive index for broadband elimination of Fresnel reflection." nature photonics **1**: 176-179.

Xiu, Y., L. Zhu, et al. (2007). "Hierarchical silicon etched structures for controlled hydrophobicity/superhydrophobicity." Nano Letters **7**(11): 3388-3393.

Biomimetics Learning from Nature

Edited by Amitava Mukherjee

ISBN 978-953-307-025-4
Hard cover, 534 pages
Publisher InTech
Published online 01, March, 2010
Published in print edition March, 2010

Nature's evolution has led to the introduction of highly efficient biological mechanisms. Imitating these mechanisms offers an enormous potential for the improvement of our day to day life. Ideally, by bio-inspiration we can get a better view of nature's capability while studying its models and adapting it for our benefit. This book takes us into the interesting world of biomimetics and describes various arenas where the technology is applied. The 25 chapters covered in this book disclose recent advances and new ideas in promoting the mechanism and applications of biomimetics.

InTech Europe
University Campus STeP Ri
Slavka Krautzeka 83/A
51000 Rijeka, Croatia
Phone: +385 (51) 770 447
Fax: +385 (51) 686 166
www.intechopen.com

InTech China
Unit 405, Office Block, Hotel Equatorial Shanghai
No.65, Yan An Road (West), Shanghai, 200040, China
中国上海市延安西路65号上海国际贵都大饭店办公楼405单元
Phone: +86-21-62489820
Fax: +86-21-62489821

IntechOpen